

Observation of Ultraslow Shock Waves in a Tunable Magnetic Lattice

Jian Li¹, S Chockalingam², and Tal Cohen^{1,3,*}

¹*Department of Civil and Environmental Engineering, Massachusetts Institute of Technology, Cambridge, Massachusetts 02139, USA*

²*Department of Aeronautics and Astronautics, Massachusetts Institute of Technology, Cambridge, Massachusetts 02139, USA*

³*Department of Mechanical Engineering, Massachusetts Institute of Technology, Cambridge, Massachusetts 02139, USA*



(Received 29 January 2021; accepted 20 May 2021; published 29 June 2021)

The combination of fast propagation speeds and highly localized nature has hindered the direct observation of the evolution of shock waves at the molecular scale. To address this limitation, an experimental system is designed by tuning a one-dimensional magnetic lattice to evolve benign waveforms into shock waves at observable spatial and temporal scales, thus serving as a “magnifying glass” to illuminate shock processes. An accompanying analysis confirms that the formation of strong shocks is fully captured. The exhibited lack of a steady state induced by indefinite expansion of a disordered transition zone points to the absence of local thermodynamic equilibrium and resurfaces lingering questions on the validity of continuum assumptions in the presence of strong shocks.

DOI: [10.1103/PhysRevLett.127.014302](https://doi.org/10.1103/PhysRevLett.127.014302)

The propagation of shock waves in solids has received enormous attention in the last several decades [1–4]. Experiments, molecular dynamic simulations, and continuum mechanics modeling have been performed to investigate shock waves [5–8] and their interactions with complex material response such as plasticity [9], damage [10], dislocation and twinning [11–13], and phase transformation [14–16]. However, the microscopic mechanisms behind their formation are yet to be fully understood.

Since the first development of modern shock wave theory, it is widely accepted that, at the continuum scale, shock waves can be modeled as steadily propagating discontinuities within a medium [17]. While it is acknowledged that, in a physical system, even vanishing levels of viscosity or rate sensitivity promote a continuous waveform, the thickness of this wave is thought to be steady and infinitesimal compared to the scale of the continuum process [18]. Hence, the main features of shock wave propagation can be captured using one-dimensional rate-independent theories [19]. However, over the years, there have been indications of situations in which these assumptions break down [20–24]. Since the macroscopic response of a solid is intrinsically linked to its response at the microscopic scale, it is plausible that in these situations additional information on the microscopic process occurring within the narrow region of the shock is needed to explain the continuum level observations. However, to the best of our knowledge, the evolution and propagation of shock waves at the molecular scale has only been captured via numerical simulations [24–26]; whereas their direct observation can serve to better elucidate shock wave phenomena and to distinguish between artifacts of numerical modeling and the actual physics.

Packed granular chains serve as an example discrete system, which has been extensively studied due to its ability to generate strongly nonlinear waves, including shock waves [27] and Nesterenko solitary waves [28]. In these chains, the Hertzian contact between particles leads to their deformation in a highly nonlinear process, which is also responsible for significant energy dissipation. The response of these systems is thus not directly comparable to molecular-scale phenomena.

To mimic the molecular-scale response, we develop a desktop-scale experimental realization of shock wave evolution in a tunable magnetic lattice. We demonstrate the propagation of strong shocks and capture their entire evolution from a benign wave. Our validated numerical model provides a comprehensive understanding of the observed phenomena and its sensitivity to both external damping and the imposed waveform. Moreover, it confirms that this system supports the propagation of quasisteady strong shocks, in which the shock front exhibits “soliton-like” features propagating at constant velocity and strength, while the particle velocity profile reaches a steady oscillatory state. It is shown that for strong shocks a highly disordered transition regime emerges, from the shock front to the steady oscillatory state, and expands indefinitely, thus revealing an unsteady feature of shock waves that nucleates at the molecular scale and can grow to the macroscopic scale.

To realize shock wave evolution that is comparable to a molecular-scale process, but in a desktop-scale system, the experimental setup requires a tunable lattice with minimal levels of dissipation. Provided a finite imaging window, the system should evolve a benign impact into a shock within a prescribed propagation distance and at sufficiently slow velocities. The former can be achieved by particles with

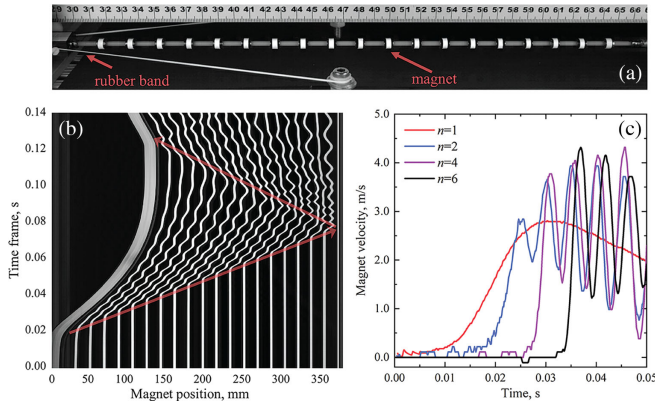


FIG. 1. Experimental setup and representative results with initial magnet separation $r_0 = 12$ mm. (a) Experimental system consisting of magnet lattice threaded on a rigid rod. The impact pulse wave is generated by releasing the left magnet. (b) Magnet trajectories are shown as white curves, by vertically stacking images of the system at different times. (c) Magnet particle velocity profiles reconstructed via digital image correlation.

highly nonlinear repelling forces (i.e., strongly convex force-separation curve) and the latter by tuning the stiffness-to-mass ratio (i.e., the ratio between the local slope of the force-separation curve and the particle mass). To meet these requirements, we take advantage of the highly nonlinear repelling nature of rare-Earth magnets and construct a lattice of 21 particles with outer diameter of 6.35 mm, length of 6.35 mm, and mass of $m = 1.084$ g, as shown in Fig. 1(a). The magnets are free to slide on a nonmagnetic, minimal friction, supporting cylindrical rod. The first magnet (on the left) is attached to two tilted prestretched rubber bands through a plastic connector, while the last magnet is fixed. The magnets are initially equispaced and preloaded to tune the repulsive force (or, equivalently, the stiffness) before impact. The imparted wave is generated by releasing the first magnet, thus allowing the rubber bands to contract and initiate the propagation [see Fig. 1(b) and Video S1 [29]]. The dynamic process is recorded by a high-speed camera (Photron SA5, 1280×800 pixels) at 8 kHz, allowing the measurement of magnet displacement, velocity, and acceleration via digital image correlation method. Using this setup the impact strengths and lattice stiffness are separately tuned by varying the prestretch of the rubber bands or the initial separation between the magnets, respectively. More details of the experimental system are given in Sec. S1 of the Supplemental Material [29].

To show that this system is capable of evolving an ordinary waveform into a shock, within the allocated propagation distance, we examine its response to an impact. The magnet trajectories are shown in Fig. 1(b) for the case with maximum impact velocity $V_I = 2.81$ m/s and with an initial magnet separation of $r_0 = 12$ mm. As indicated by the red arrow, the evolution of the magnet displacements

shows a wave propagating from the impacted end, into the lattice at $V_P = 6.42$ m/s. Then, upon arrival at the last magnet, a reflection wave propagates back. It is seen from the displacement profiles that, although the imparted waveform is smooth, its propagation induces sharp oscillations in magnet particle displacement curves, indicating rapid changes in magnet velocities.

If a shock forms, the wave profile is expected to steepen. By examining the velocity profiles of different magnet particles in Fig. 1(c), it is clearly observed that in our system significant steepening occurs and is accompanied by oscillations that become more violent as propagation proceeds. In particular, notice the decreasing rise times (i.e., the duration from zero velocity to first peak velocity), which reduce from 23.9 ms for the first particle ($n = 1$) to 4.9 ms for $n = 6$. This result clearly demonstrates the realization of a longitudinal shock wave and its evolution from a simple wave. Moreover, the violent oscillations of increasing amplitude, in what seems to be a highly disordered process, are indicative of strong shocks.

To better understand the observed shock evolution, we numerically model the system as a chain of particles connected by nonlinear springs. In the following analysis, we only consider the interaction between first neighboring magnets. Although some influence may arise from the magnetic field of the non-nearest particles, it is a second-order effect (see Sec. S3 in the Supplemental Material [29]). Additionally, we neglect magnet rotations, and the length of the magnet is not considered in the calculation of propagation velocity. Accordingly, the equation of motion for the n th magnet reads

$$m \frac{d^2 u_n}{dt^2} = F_{n-1} - F_n - f_n, \quad (1)$$

where u_n denotes the particle displacement, and F_n and f_n are the repulsive and frictional forces, respectively. In particular, based on experimental measurement of the force-displacement curve [Fig. 2(a)], the repulsive force is approximated using the formula $F = K/(r + b)^q$, where r is the separation between two neighbor particles, and the coefficient values are $K = 413.8$ N mm³, $b = 3.917$ mm, and $q = 3$. A Coulomb model captures the influence of friction between the rod and the magnets via the formula $f_n = \mu[mg + p(F_{n-1} + F_n)]$, where the coefficients $\mu = 0.285$ and $p = 0.012$ are experimentally calibrated (see Supplemental Material Sec. S4 [29]), and g is the gravitational acceleration. The measured motion of the impacting magnet $u_1(t)$ is given as a boundary condition at one end, while at the other end we impose $u_{21}(t) = 0$. The equations of motion are numerically solved using a finite-difference method [32]. Numerical results obtained using this model are compared with experimental curves for the second and eighth magnets in Figs. 2(b)–2(e) and show excellent agreement for the velocity profiles. The

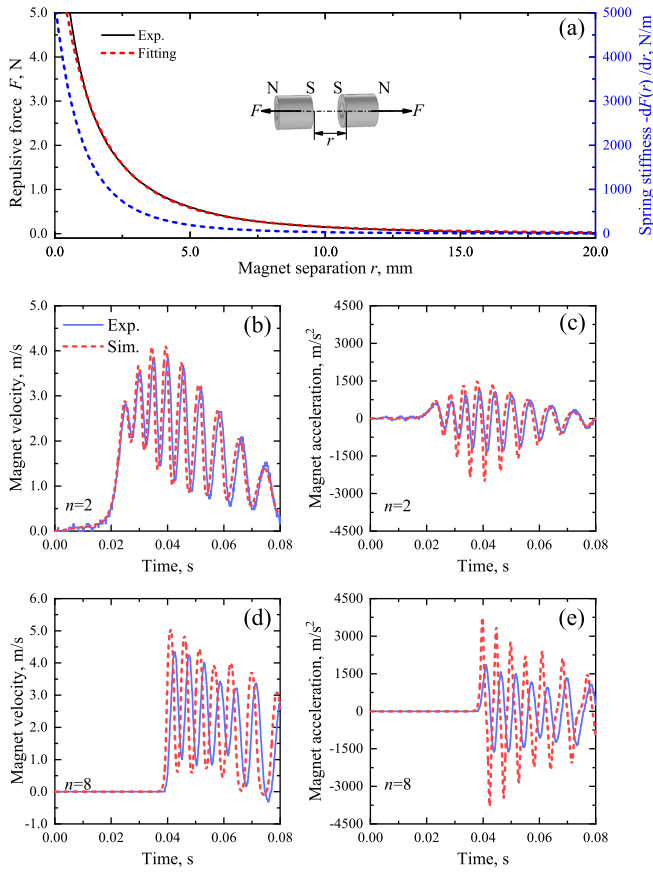


FIG. 2. Comparison of experimental and numerical results. (a) Force-displacement curve and instantaneous stiffness for the nearest magnet interaction. (b)–(e) Experimental (continuous blue lines) and numerical (dashed red lines) results for magnet particle velocities and accelerations. The uncertainties in the velocity and acceleration measurements are 0.16 m/s and 170.67 m/s^2 , respectively. Details of the derivation process are shown in Sec. S2 of the Supplemental Material [29].

acceleration profiles are also well captured by the simulation. The discrepancy in peak accelerations can be explained by the limited image resolution (~ 20 pixels per ring magnet particle length), which is insufficient to capture sharp changes in acceleration (see Sec. S2 of the Supplemental Material [29]).

Next, we use our calibrated model to investigate the long-time behavior of strong shocks. For simplicity, we consider a long lattice subjected to a constant impactor velocity (a long lattice is used to avoid wave reflections). Figure 3(a) shows a typical velocity profile obtained for an impactor velocity of $V_I = 2$ m/s, in the absence of friction. Upon arrival of the shock front, the particle velocity is shown to rapidly increase to 3.87 m/s, followed by strong oscillations with a decaying amplitude. Unlike a linear system, for which the vibration amplitude decays completely (see Supplemental Material Secs. S5 and S9 [29]), a stable finite-amplitude oscillation about the impactor velocity is eventually attained. Note that this motion is

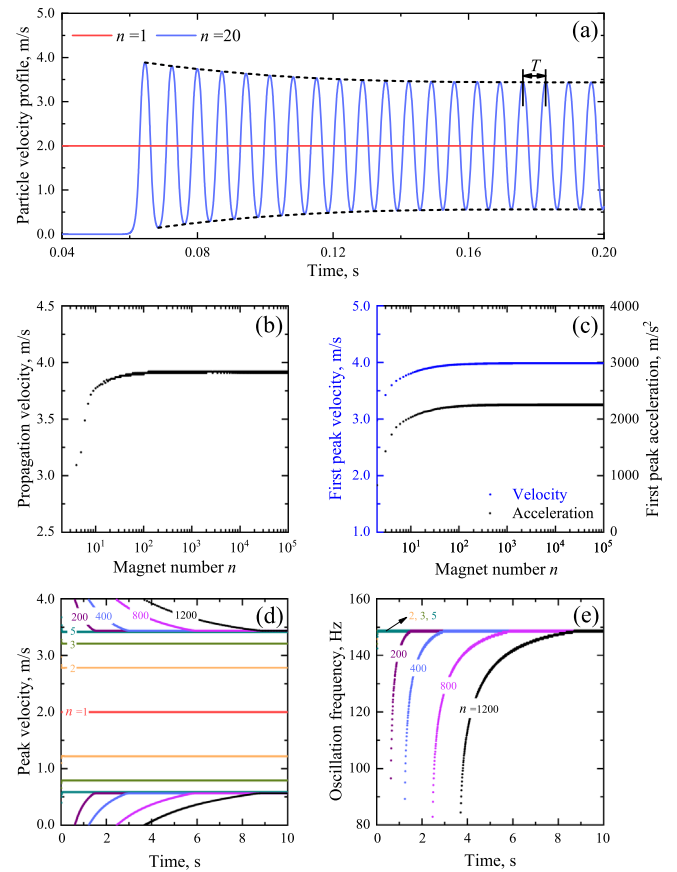


FIG. 3. Long-time dynamic response of the system without friction. (a) Typical velocity profile of a particle. (b) Variation of propagation velocity as the wave progresses through particles into the lattice. (c) First peak velocity and first peak acceleration of each particle. (d) Evolution of peak velocity (both local maximum and minimum peaks) with time for various particles. (e) Evolution of oscillation frequency with time for various particles. Results are shown for the system with initial separation $r_0 = 12$ mm.

nonharmonic due to the nonlinearity of the system. Examining the corresponding propagation velocity of the shock front in Fig. 3(b), we show that it gradually approaches a constant value of $V_p = 3.92$ m/s. It is notable that this stabilized propagation velocity is significantly larger than the impactor velocity and the linear propagation velocity $V_0 = 1.62$ m/s [33]. If frictional effects are included, a gradual decay of the propagation velocity is expected beyond a peak value (see Sec. S6 in the Supplemental Material [29]). Nonetheless, once developed, the early-time propagation velocity (i.e., for the first ~ 20 magnets) is comparable to the propagation velocity in the frictionless system. Figure 3(c) shows that both the first peak velocity and the first peak acceleration increase with increasing particle number, which is an intrinsic feature of strong shock waves. Eventually, the competition between nonlinearity and dispersion in the system results in

saturation of the first peak velocity and peak acceleration. In particular, the saturated first peak velocity is $2V_I$.

Further, to understand the transition from the wave front to the stabilized oscillatory state, Figs. 3(d) and 3(e) present the peak velocity and the corresponding oscillation frequency for different particle numbers as a function of time. We find that both the amplitude and the period decrease with time; moreover, after a rapid increase in stabilized oscillation amplitude (from the first magnet to the fifth magnet), the following particles arrive at the same oscillatory state (same amplitude and same period). Nonetheless, it is observed that the time of transitioning from peak velocity to the stabilized state is longer for the larger particle numbers, resulting in the highly disordered transition zone that expands indefinitely as the shock front penetrates deeper into the undisturbed lattice (see Video S2 [29]). Analogous to the interpretation of molecular-scale response, the finite-amplitude steady oscillation in the wake of a shock is consistent with an increase in temperature [34], whereas the disordered transition region appears to be out of thermodynamic equilibrium and its growth can be attributed to increasing entropy.

To further understand the range of shock wave response realized in our experiments, we explore the effect of the impactor velocity on the propagation velocity of the quasisteady shock wave in Fig. 4(a). The nearly linear dependence observed in both experimental and numerical results resembles the reported experimental findings of shock Hugoniot data in metallic materials [35] and molecular simulations of shock waves [36]. The agreement between theory and experiments is shown with slight deviations attributed primarily to effects of friction and the precise form of the imparted wave that is neglected in the simulation (see Supplemental Material Secs. S6 and S7 [29]). While these curves, as well as the corresponding oscillation frequency [Fig. 4(b)], do not reveal information on the shock strength, we examine in Fig. 4(c) the kinetic energy associated with the steady-state oscillation. Quite noticeably, the increase in oscillation energy becomes pronounced beyond a critical impactor velocity V^* , which is smaller than the linear propagation velocity (i.e., $V^* < V_0$). This threshold velocity represents the transition into the strong shock regime, which is characterized by a dramatic increase in energetic consumption.

In the absence of a unified quantitative definition of strong shocks, which are typically distinguished from weak and moderate shocks by virtue of the *very large* magnitude jump in field variables that they impose [37], here we propose a quantitative definition of strong shocks based on the oscillation energy ratio, which is directly linked to the level of energy dissipation. We identify the critical impact velocity V^* for the onset of a strong shock as velocity at which the curvature of the oscillation energy ratio curve changes sign, namely $d^2\eta/dV_I^2 = 0$ [see inset in Fig. 4(d)]. Accordingly, strong shocks occur for $V_I > V^*$, and

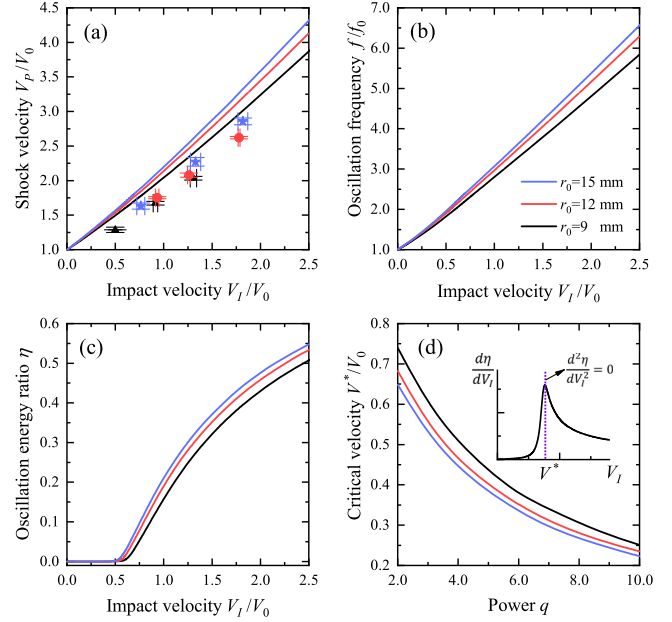


FIG. 4. Dependence of the stabilized shock response on impactor velocity. Curves represent numerical solutions. Experimental data are shown as colored markers with error bars. (a) Shock wave propagation velocity. (b) Stabilized oscillation frequency f . (c) Oscillation energy ratio η . (d) Critical velocity. Here f_0 represents the linear oscillation frequency, defined as $f_0 = 1/\pi \sqrt{-(1/m)dF(r)/dr|_{r=r_0}}$, and $\eta = 1/T \int_{t_0}^{t_0+T} [V(t)/V_I - 1]^2 dt$, where $T = 1/f$. If the oscillation is harmonic, $\eta = 0.5$.

moderate shocks occur in the finite range $V_I \in (0, V^*)$. A weak shock appears at the limit $V_I \rightarrow 0$ [38]. From this definition it is clear that strong shocks are observed in our experiments [see Fig. 4(a)]. Moreover, despite the 8 orders of magnitude difference in length scale, the desktop-scale magnet lattice system preserves the key quantitative features of shock wave propagation in an analogous atomic system (as compared to a copper atomic lattice in Sec. S8 of the Supplemental Material [29]).

In Fig. 4(d), we further investigate this critical threshold by examining the influence of the stiffening law or, in particular, the power q . We observe that a system with increased stiffening can be driven beyond the critical threshold by lower impactor velocities.

In conclusion, we have shown that the desktop-scale experimental system presented here allows for complete spatiotemporal capture of the evolution of strong shocks from benign imparted waveforms. This is facilitated by taking advantage of the highly nonlinear repelling force between neighboring rare-earth magnets in a tunable one-dimensional lattice. Comprehensive investigation of the lattice response uncovers behaviors of strong shocks, which agree with predictions from molecular dynamic simulations. Hence, this Letter gives rise to a new avenue for

investigation of shock wave phenomena at the microscopic scale. Moreover, through this analysis, we observe the formation of a highly disordered transition region in the wake of strong shocks. This region nucleates at the particle scale, but continues to grow indefinitely. Observation of this phenomena at the macroscale, raises questions on the validity of continuum assumptions in the presence of strong shocks. Future work can take advantage of this system to expand beyond uniaxial propagation and can include additional physical effects, such as structure defects, thermal vibrations, and dissipation. Moreover, it is worth mentioning that the current design could also be modified to explore other nonlinear wave phenomena, such as solitons [39–41], elastic band gaps [42], and nonreciprocal waves [43–45].

The authors wish to acknowledge the financial support of the Army Research Office, under Grant No. W911NF-19-1-0275 and support from the National Science Foundation (CMMI, MOMS, 1942016).

*Corresponding author.
talco@mit.edu

- [1] R. McQueen and S. Marsh, Equation of state for nineteen metallic elements from shock-wave measurements to two megabars, *J. Appl. Phys.* **31**, 1253 (1960).
- [2] B. L. Holian and P. S. Lomdahl, Plasticity induced by shock waves in nonequilibrium molecular-dynamics simulations, *Science* **280**, 2085 (1998).
- [3] Y. Yao, Z. Huang, P. Xie, L. Wu, L. Ma, T. Li, Z. Pang, M. Jiao, Z. Liang, J. Gao *et al.*, High temperature shockwave stabilized single atoms, *Nat. Nanotechnol.* **14**, 851 (2019).
- [4] S. A. Simmons, F. A. Bayocboc, Jr., J. C. Pillay, D. Colas, I. P. McCulloch, and K. V. Kheruntsyan, What is a Quantum Shock Wave? *Phys. Rev. Lett.* **125**, 180401 (2020).
- [5] S. Catheline, J.-L. Gennisson, M. Tanter, and M. Fink, Observation of Shock Transverse Waves in Elastic Media, *Phys. Rev. Lett.* **91**, 164301 (2003).
- [6] D. Espíndola, S. Lee, and G. Pinton, Shear Shock Waves Observed in the Brain, *Phys. Rev. Applied* **8**, 044024 (2017).
- [7] S. Chockalingam and T. Cohen, Shear shock evolution in incompressible soft solids, *J. Mech. Phys. Solids* **134**, 103746 (2020).
- [8] K. T. Ramesh, High rates and impact experiments, in *Springer Handbook of Experimental Solid Mechanics*, edited by W. N. Sharpe (Springer US, Boston, MA, 2008), pp. 929–960.
- [9] M. Chen, J. McCauley, D. Dandekar, and N. Bourne, Dynamic plasticity and failure of high-purity alumina under shock loading, *Nat. Mater.* **5**, 614 (2006).
- [10] S. Fensin, J. Escobedo, G. Gray III, B. Patterson, C. Trujillo, and E. Cerreta, Dynamic damage nucleation and evolution in multiphase materials, *J. Appl. Phys.* **115**, 203516 (2014).
- [11] A. Higginbotham, M. J. Suggit, E. M. Bringa, P. Erhart, J. A. Hawreliak, G. Moggi, N. Park, B. A. Remington, and J. S. Wark, Molecular dynamics simulations of shock-induced deformation twinning of a body-centered-cubic metal, *Phys. Rev. B* **88**, 104105 (2013).
- [12] C. Wehrenberg, D. McGonegle, C. Bolme, A. Higginbotham, A. Lazicki, H. Lee, B. Nagler, H.-S. Park, B. Remington, R. Rudd *et al.*, In situ x-ray diffraction measurement of shock-wave-driven twinning and lattice dynamics, *Nature* **550**, 496 (2017).
- [13] S. J. Turneaure, P. Renganathan, J. M. Winey, and Y. M. Gupta, Twinning and Dislocation Evolution during Shock Compression and Release of Single Crystals: Real-Time X-Ray Diffraction, *Phys. Rev. Lett.* **120**, 265503 (2018).
- [14] G. Duvall and R. Graham, Phase transitions under shock-wave loading, *Rev. Mod. Phys.* **49**, 523 (1977).
- [15] K. Kadau, T. C. Germann, P. S. Lomdahl, and B. L. Holian, Microscopic view of structural phase transitions induced by shock waves, *Science* **296**, 1681 (2002).
- [16] N. Amadou, T. de Resseguier, A. Dragon, and E. Brambrink, Coupling between plasticity and phase transition in shock-and ramp-compressed single-crystal iron, *Phys. Rev. B* **98**, 024104 (2018).
- [17] M. D. Salas, The curious events leading to the theory of shock waves, *Shock Waves* **16**, 477 (2007).
- [18] R. Courant and K. Friedrichs, *Supersonic Flow and Shock Waves* (Interscience, New York, 1948).
- [19] T. Von Karman and P. Duwez, The propagation of plastic deformation in solids, *J. Appl. Phys.* **21**, 987 (1950).
- [20] J. Hsu and R. Clifton, Plastic waves in a rate sensitive material—i. Waves of uniaxial stress, *J. Mech. Phys. Solids* **22**, 233 (1974).
- [21] A. Molinari and G. Ravichandran, Fundamental structure of steady plastic shock waves in metals, *J. Appl. Phys.* **95**, 1718 (2004).
- [22] J. K. Knowles, Impact-induced tensile waves in a rubberlike material, *SIAM J. Appl. Math.* **62**, 1153 (2002).
- [23] J. Niemczura and K. Ravi-Chandar, On the response of rubbers at high strain rates—ii. Shock waves, *J. Mech. Phys. Solids* **59**, 442 (2011).
- [24] B. L. Holian and G. K. Straub, Molecular dynamics of shock waves in one-dimensional chains, *Phys. Rev. B* **18**, 1593 (1978).
- [25] D. H. Tsai and C. Beckett, Shock wave propagation in cubic lattices, *J. Geophys. Res.* **71**, 2601 (1966).
- [26] B. L. Holian and G. K. Straub, Molecular Dynamics of Shock Waves in Three-Dimensional Solids: Transition from Nonsteady to Steady Waves in Perfect Crystals and Implications for the Rankine-Hugoniot Conditions, *Phys. Rev. Lett.* **43**, 1598 (1979).
- [27] A. Molinari and C. Daraio, Stationary shocks in periodic highly nonlinear granular chains, *Phys. Rev. E* **80**, 056602 (2009).
- [28] V. F. Nesterenko, Propagation of nonlinear compression pulses in granular media, *J. Appl. Mech. Tech. Phys.* **24**, 733 (1983).
- [29] See Supplemental Material at <http://link.aps.org/supplemental/10.1103/PhysRevLett.127.014302> for more details on (S1) experimental details, (S2) estimation of uncertainty in velocity and acceleration derivation, (S3) measurement of the magnetic interaction force, (S4) calibration of the Coulomb friction coefficient, (S5) dynamic

- response of a linear lattice, (S6) effect of friction on propagation velocity, (S7) effect of loading profile in the nonlinear system, (S8) quantitative comparison of magnetic system and copper atom lattice, and (S9) effect of impactor velocity on the dynamic response of the nonlinear system, which includes Refs. [30,31].
- [30] C. Robbe, N. Nsiampa, A. Oukara, and A. Papy, Quantification of the uncertainties of high-speed camera measurements, *Int. J. Metrol. Qual. Eng.* **5**, 201 (2014).
- [31] Ş. Erkoç, Empirical potential energy functions used in the simulations of materials properties, *Annu. Rev. Comput. Phys.* **IX**, 1 (2001).
- [32] R. J. LeVeque, *Finite Difference Methods for Ordinary and Partial Differential Equations: Steady-State and Time-Dependent Problems* (SIAM, Philadelphia, 2007).
- [33] Here, the linear velocity refers to the propagation velocity of small amplitude disturbances, which can be calculated as $V_0 = r_0 \sqrt{-(1/m)dF(r)/dr|_{r=r_0}}$, where r_0 represents the initial magnet separation.
- [34] G. K. Straub, B. L. Holian, and R. G. Petschek, Molecular dynamics of shock waves in one-dimensional chains. ii. Thermalization, *Phys. Rev. B* **19**, 4049 (1979).
- [35] S. P. Marsh, *LASL Shock Hugoniot Data* (University of California Press, Berkeley, 1980), Vol. 5.
- [36] T. Hill and L. Knopoff, Propagation of shock waves in one-dimensional crystal lattices, *J. Geophys. Res.* **85**, 7025 (1980).
- [37] R. Courant and K. O. Friedrichs, *Supersonic Flow and Shock Waves*, Applied Mathematical Sciences Vol. 21 (Springer Science & Business Media, New York, 1999).
- [38] Weak shocks are simple waves up to second-order approximation in the shock strength [37].
- [39] B. Deng, J. R. Raney, V. Tournat, and K. Bertoldi, Elastic Vector Solitons in Soft Architected Materials, *Phys. Rev. Lett.* **118**, 204102 (2017).
- [40] B. Deng, C. Mo, V. Tournat, K. Bertoldi, and J. R. Raney, Focusing and Mode Separation of Elastic Vector Solitons in a 2d Soft Mechanical Metamaterial, *Phys. Rev. Lett.* **123**, 024101 (2019).
- [41] Y. Zhang, B. Li, Q. Zheng, G. M. Genin, and C. Chen, Programmable and robust static topological solitons in mechanical metamaterials, *Nat. Commun.* **10**, 5605 (2019).
- [42] B. Deng, P. Wang, Q. He, V. Tournat, and K. Bertoldi, Metamaterials with amplitude gaps for elastic solitons, *Nat. Commun.* **9**, 3410 (2018).
- [43] Y. Wang, B. Yousefzadeh, H. Chen, H. Nassar, G. Huang, and C. Daraio, Observation of Nonreciprocal Wave Propagation in a Dynamic Phononic Lattice, *Phys. Rev. Lett.* **121**, 194301 (2018).
- [44] H. Nassar, B. Yousefzadeh, R. Fleury, M. Ruzzene, A. Alù, C. Daraio, A. N. Norris, G. Huang, and M. R. Haberman, Nonreciprocity in acoustic and elastic materials, *Nat. Rev. Mater.* **5**, 667 (2020).
- [45] M. Brandenbourger, X. Locsin, E. Lerner, and C. Coullais, Non-reciprocal robotic metamaterials, *Nat. Commun.* **10**, 4608 (2019).